Spectrum Analysis of 2-D Plasmon in GaN-Based High Electron Mobility Transistors

Lin Wang, Xiao-Shuang Chen, Wei-Da Hu, and Wei Lu, *Member, IEEE*

***Abstract*—We have investigated terahertz (THz) resonant absorption spectra in grating-gate GaN high electron mobility transistors. The results indicate that both the symmetrical plasmon mode and the asymmetrical plasmon mode play an important role in the strong absorption of THz waves. The excitation process and dynamic response of these plasmons are investigated in detail. Our results also indicate that the asymmetrical plasmon is induced by the surface polarization field of the electrodes and the resonant strength of this plasmon is reduced significantly by the decay of the polarization field. Variations in the resonant strength of the plasmonic peaks are consistent with the surface resonant layer model showing that the method we used can be utilized for the study of coupling between THz radiation and plasmons in the channel. In order to achieve wider tunability, more advanced device structures can be explored such as a device that contains double channel layers, in which complicated plasmons can be excited.**

***Index Terms*—High electron mobility transistors (HEMTs), plasmonics, spectrum, terahertz (THz) detectors.**

I. Introduction

In THE last decade, voltage tunable solid-state detectors have gained wide recognition as potential devices for the realization of integrated terahertz (THz) electronics in many technological applications such as imaging/sensing systems, communication systems, etc. [1]–[3]. Since the first demonstration of 2-D plasmon resonance in a submicron high electron mobility transistor (HEMT) with an operating frequency located in the THz range, various theoretical and experimental studies on THz wave resonances have been performed [4]–[8]. In principle, 2-D plasmons behave like shallow water under a gate, and the fundamental frequency of the plasmonic oscillations is determined by the gate length and plasma wave velocity. Hydrodynamic nonlinearity of plasmonic oscillations can cause a constant source-to-drain voltage, which is recognized as a photoresponse under the illumination of the HEMT by THz waves. In the region of off-resonance, the photoresponse is a smooth function of gate voltage as well as frequency [9], [10], while resonant photoresponse can be obtained if certain conditions are satisfied [11].

However, short gated plasmons couple very poorly to THz radiation due to the acoustical nature and small net dipole moment of these plasmons [12]. The observed resonant structures in the photoresponse are mainly caused by the nonlinearity of gated plasmons [13]. Although previous electrostatic theories can predict relatively accurate results for the frequencies of THz resonance, the effective excitation of plasmonic resonance and the broadening of spectral peaks still need to be explained [14], [15]. Popov *et al*. have shown that the broadening of a gated plasmon resonance linewidth is mainly caused by the intermodal plasmon–plasmon scattering (the process during which the resonant gated plasmons excite the nonresonant ungated plasmons) at the ends of the gated portion of the transistor channel [16]. Special antennas are needed to improve the efficiency of coupling between the THz radiation and gated plasmons. In previous work, metal grating-gate transistors for both THz emission and detection have been proposed [8], [17], [18]. There are two purposes for using a grating-gate coupler: one is the spatial modulation of electron density, and the other is for the excitation of 2-D plasmons through a spatially modulated THz near-field/polarization field. Most of the reported works focus on GaAs HEMTs with submicrometer gate length due to the low electron density in the channel.

Recently, large area slit grating-gate GaN HEMTs have attracted much attention for the potential of wide tunability in the THz frequency domain due to high electron density induced by the polarization effect [18]–[20]. In this paper, THz resonant absorption in GaN HEMTs with metal grating-gate and quantum-wire grating-gate structures are investigated in detail. The field distributions and dipole oscillations of plasmons in the single electron layer are presented for better understanding about the dynamic of plasmonic oscillation.

II. Device Description and Characteristic Parameters

Fig. 1 shows the typical structure of a grating-gate GaN HEMT. The device epilayer structures are grown by low-pressure metal organic chemical vapor deposition on 4H-SiC or sapphire substrates [21]. All the AlGaN and GaN layers are assumed to be Ga face. The thickness of the $Al_xGa_{1-x}N$ buffer layer is usually in the range of 1–2 μm in order to ensure high crystal quality. However, the mole fraction x should not exceed 15%, because a larger mole fraction can lead to severe interface scattering and depletion of the 2-D electron gas

Manuscript received September 22, 2011; revised December 2, 2011, December 30, 2011, and February 4, 2012; accepted February 9, 2012. Date of publication February 17, 2012; date of current version February 1, 2013. This work was supported in part by the State Key Program for the Basic Research of China under Grant 2007CB613206 and Grant 2011CB922004, by the National Natural Science Foundation of China under Grant 61006090, Grant 10725418, Grant 10734090, Grant 10990104, and Grant 60976092, and by the Fund of Shanghai Science and Technology Foundation under Grant 09DJ1400203, Grant 09dz2202200, Grant 10JC1416100, and Grant 10510704700, and the Knowledge Innovation Program of the Chinese Academy of Sciences under Grant Q-ZY-7.

The authors are with the National Laboratory for Infrared Physics, Shanghai Institute of Technical Physics, Chinese Academy of Sciences, Shanghai 200083, China (e-mail: xschen@mail.sitp.ac.cn; wdhu@mail.sitp.ac.cn).

Color versions of one or more of the figures in this paper are available online at http://ieeexplore.ieee.org.

Digital Object Identifier 10.1109/JSTQE.2012.2188381

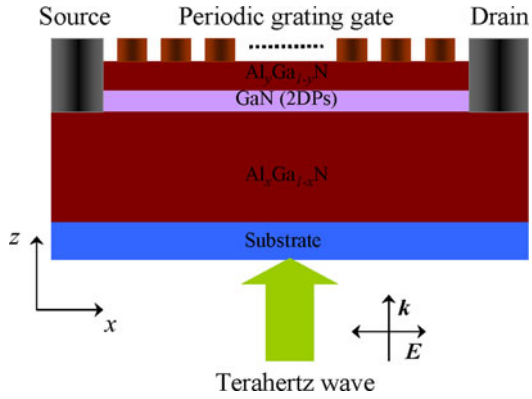

Fig. 1. Device cross section: the THz wave is incident from bottom of substrate with linear polarization electric field $\boldsymbol{E}$ and wave vector $\boldsymbol{k}$.

(2DEG) in the GaN channel layer. After the buffer layer, the GaN channel and the $Al_yGa_{1-y}N$ barrier are sequentially grown with a thickness of approximately 30 nm. The mole fraction y in $Al_yGa_{1-y}N$ barrier is approximately 30%. Transistor fabrication can be completed after the deposition of electrodes. The measured room temperature Hall mobility and sheet electron density are approximately 1200 cm^{-2}/V·s and 1–3 $\times 10^{13}$ cm^{-2}, respectively [21]. A TM polarization THz wave is incident from the backside of the device (our results indicate that stronger absorption can be obtained when the THz wave is incident from backside, see Fig. 4 and discussions therein). As mentioned earlier, due to the small net dipole moment of gated plasmons, a grating coupler is required to improve the coupling efficiency. The coupler, also serving as electrodes [18], can be formed by electron-beam etching. The period of the grating gate is 0.6 μm. A 0.7 duty cycle is implemented to ensure uniformity of the 2-D channel. Thus, the interaction between gated and ungated plasmons can be neglected.

III. Analysis Model and Simulations

The plasma wave behavior in a HEMT can be described by the hydrodynamic equations as follows [4]:

$$\frac{\partial \boldsymbol{v}}{\partial t} + (\boldsymbol{v}\cdot\nabla)\boldsymbol{v} = -\frac{e}{m^*}\boldsymbol{E} - \frac{\boldsymbol{v}-\boldsymbol{v}_{\rm dr}}{\tau} \quad \text{(Euler equation)} \quad (1)$$

$$\frac{\partial n}{\partial t} + \nabla(n\boldsymbol{v}) = 0 \quad \text{(Continuity equation)} \quad (2)$$

where m^* denotes the effective mass of an electron, about $0.2m_0$ in GaN (m_0 is free electron mass), $\boldsymbol{E}$ is the oscillating electric field along the channel, and τ is the electron relaxation time ($\tau = \mu m^*/e$), in our case $\tau = 1.7 \times 10^{-13}$ s. $\boldsymbol{v}$ and $\boldsymbol{v}_{\rm dr}$ are the electron velocity under THz electromagnetic field and dc biases, respectively. For a grating-gated single channel system, the electromagnetic coupling of plasmonic oscillations between neighboring regions may not be neglected, which is different from single gate system. The induced-oscillating current not only relies on the local electric field, but also on the electric field in other regions (spatial dispersion). The general linear expression for an electric current induced by an oscillating electric field (angular frequency ω) along the channel is

$$\boldsymbol{j}(x,z,\omega) = \int_{-\infty}^{+\infty} \sigma(x,x',\omega)\boldsymbol{E}(x',z,\omega)\mathrm{d}x' \quad (3)$$

where the kernel $\sigma(x,x',\omega)$ describes the spatial dispersion in the 2-D electron system. In a spatially periodic system with period a along the x-direction, the electric field can be expressed as follows:

$$\boldsymbol{E}(x,z,\omega) = \sum_{m=-\infty}^{+\infty} \boldsymbol{E}_m(z)e^{iq_m x - i\omega t} \quad (4)$$

where $q_m = 2\pi m/a$ is an in-plane wave vector, and $\boldsymbol{E}_m(z)$ is the amplitude of the Fourier harmonic of the electric field. The total current can be expressed as the sum of currents induced by these Fourier harmonics:

$$\boldsymbol{j}(x,z,\omega) = \sum_{m=-\infty}^{+\infty} \sigma_m \boldsymbol{E}_m(z)e^{iq_m x - i\omega t}. \quad (5)$$

After linearizing the continuity and Euler's equations for the electron density n and velocity $\boldsymbol{v}$, the formulation of conductivity can be expressed as follows [22], [23]:

$$\sigma_m = \frac{n_s e^2}{m^*}\frac{i\omega}{(\omega - q_m\boldsymbol{v}_{\rm dr})(\omega - q_m\boldsymbol{v}_{\rm dr} + i\tau^{-1})} \quad (6)$$

where n_s is equilibrium electron density in the channel. The conductivity in (6) is the most important parameter and describes both plasma wave damping and plasma wave dynamics. The spatial dispersion of conductivity is related to the dc electron drift by the two parameters q_m and $\boldsymbol{v}_{\rm dr}$. In our case, the drift velocity is zero and the conductivity can be simplified by the Drude-optical conductivity [18], [24].

To examine energy transformation in the resonant surface layer (grating gated 2-D channel), the phenomenological model is used as in [24] and [25]. The admittance of the resonant surface layer is given as follows:

$$Y_{\rm eff} \sim \sum_{m=0}^{\infty} \frac{1}{\omega^2 - \omega_{pm}^2 - 2i\gamma_e\omega}. \quad (7)$$

In the neighborhood of the mth THz resonance, the transmittance and absorbance of the system can be expressed as follows:

$$T_m(\omega) \approx T_0 \frac{(\omega-\omega_{pm})^2 + \gamma_e^2}{(\omega-\omega_{pm})^2 + (\gamma_e+\gamma_{rm})^2} \quad (8)$$

$$A_m(\omega) \approx \frac{2\gamma_e\gamma_{rm}(1-\sqrt{R_0})}{(\omega-\omega_{pm})^2 + (\gamma_e+\gamma_{rm})^2} \quad (9)$$

where $\gamma_e = 1/2\tau$ is plasmon dissipative damping , γ_{rm} is proportional to the electron density n_s describing the radiative broadening of the THz resonance, and ω_{pm} denotes the mth plasmonic resonant frequency. The total broadening of the resonant line is determined by γ_e and γ_{rm}. Additionally, T_0 and R_0 are the transmissivity and reflectivity of the system when there is no resonant surface layer at the interface between the medium above and below the resonant surface layer. The maximum value of absorbance occurs at $\gamma_{rm} = \gamma_e$, approximately

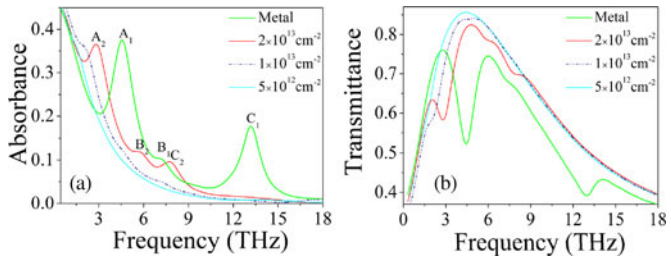

Fig. 2. Absorption and transmission spectra of quantum wire and metal wire grating-gate HEMTs: (a) absorption spectra and (b) transmission spectra of the two kind grating HEMTs with 2DEG density in quantum-wire varying from 5×10^{12} cm^{-2} to 2×10^{13} cm^{-2}. The sheet electron density in the channel is 2×10^{13} cm^{-2}. Three absorption peaks of metal/quantum wire structure are marked with A (A_1/A_2), B (B_1/B_2), and C (C_1/C_2), respectively.

$0.5(1 - \sqrt{R_0})$. To understand more clearly the physical mechanisms of the interaction between electromagnetic field and 2-D plasmons, the dynamic response of a plasma wave under irradiation by a THz wave is numerically calculated based upon the finite differential time-domain (FDTD) method [26].

IV. Results and Discussions

Either quantum wire or metal wire can be used for a grating coupler. The former has previously been proposed for THz emitter in order to be matched to frequency of plasma wave excited in the channel and improve the mode conversion gain [6]. For a THz detector, it is important to achieve sufficient absorption capability in quantum wire gated HEMTs. In the numerical discussion shown in this paper, both the quantum and metal wire grating couplers are modeled for comparison purpose. The density of 2DEG in quantum wire is set at three different levels from 5×10^{12} cm^{-2} (as high as general density in the channel) to 2×10^{13} cm^{-2}.

Fig. 2(a) shows the absorption spectra of these devices under irradiation by a THz wave. The corresponding transmission spectra are shown in Fig. 2(b) simultaneously. Three absorption peaks (marked as A_1/A_2, B_1/B_2, and C_1/C_2) are clearly visible in Fig. 2(a) in the frequency domain from 1 to 18 THz. The frequencies of peaks A_1 (f_a), B_1 (f_b), and C_1 (f_c) are 4.6, 7.4, and 13.1 THz, respectively. They correspond to the three minima in the transmission spectrum in Fig. 2(b). It is found that there are strong transmission peaks near these three frequencies. The transmissivity can reach 0.85 when the sheet density of quantum wire is 5×10^{12} cm^{-2}. The continuous redshift in frequency of these resonant peaks can also be seen in Fig. 2(a) when the sheet density of quantum wire is decreased. And peak C has a larger downshift, from which one can conclude that peak C is an oscillation mode mostly relevant to the grating coupler. However, no characteristic absorption can be observed when the density is lower than 1×10^{13} cm^{-2}. The absorption and transmission are not relevant to the resonant properties of 2-D plasmons at this density. It is believed that stronger absorption peaks corresponding to the stronger oscillation of plasmons along the channel, especially when the resonant conditions are satisfied.

The snap-shots of plasmonic oscillation are shown in Fig. 3 with continuous THz wave excitation at frequencies of peaks A_1, B_1, and C_1, respectively. The plasma waves are electronic polarization waves so that they can produce an alternating electric field. The distributions of the electric field, including E_x component and E_z component, are shown in Fig. 3(a)–(f). With the help of electric field distributions, the dipole oscillations are shown by arrows in the third row of Fig. 3. The positive and negative symbols "+" and "−" indicate the depletion and accumulation of electrons, respectively. Note that, in Fig. 3(i), the charge separation is just the indication of charge density fluctuation. And the style of this plasmonic oscillation is different from that of Fig. 3(g) and (h), which can also be concluded from the E_z distribution since the E_z component orients to the same direction at two sides of the channel layer in Fig. 3(c) and orients to the opposite direction in Fig. 3(a) and (b). From this, two kinds of plasmons can be obtained: one is the symmetrical plasmon with symmetrical oscillating charge distributions across the channel layer (in respect to the central plane of channel) and another one is asymmetrical charge distribution. So, it can be concluded that the spectral peaks A_1 and B_1 are mainly caused by the excitation of symmetrical plasmon mode (SPM), and peak C_1 is caused by the excitation of asymmetrical plasmon mode (ASPM) (Note that in this paper, the finite thickness of the 2DEG layer is considered. The thickness we used is 30 nm according to the conduction band profile—the distance from heterointerface to the place where the conduction band of the buffer layer is flat. The electromagnetic interaction between carriers at two surface of the 2DEG layer can lead to the formation of ASPM plasmon. In actual transistor channel, the electron density distribution is around 10 nm (see [21]). Despite this, the common properties of resonance C are captured since that the frequency of resonance C remains unchanged if the thickness d_c varies from 30 to 10 nm. In other words, the condition $k_p d_c \ll 1$ must be satisfied so that the coupling strength between charge density oscillations at two surfaces of the 2DEG layer keeps almost unchanged, where k_p is the plasmon wave vector. And no obvious frequency shift of resonance C can be observed.). At this point, we provide the simplest way to reveal the excitation process and the dynamic response of the plasmons in single channel system, which is not given in [27]. (In [27], we mainly focus on the coupling of plasmons supported in different channels. Only the dipole distributions along the single channel layer are shown in the inset of the Fig. 2 for comparison purpose. However, the physical mechanisms and dynamics of these plasmons are not explored in detail, which deserves much attention.)

As shown in Fig. 3, the length of gate finger is approximately a multiple of the half wavelength of the SPM plasma wave. Therefore, the resonant condition is satisfied, and the absorption peaks A_1 and B_1 are caused by resonant plasmonic oscillations. The maximum value of absorbance is smaller than 0.5, which is in agreement with the resonant surface layer model in Section III. Additionally, the large difference of absorbance between peaks A_1 and B_1 in Fig. 2(a) can be explained by the distribution of the E_x component in Fig. 3. A larger net dipole moment can be found in Fig. 3(d) indicating that there is a larger energy transferred from external incident wave to 2-D plasmons.

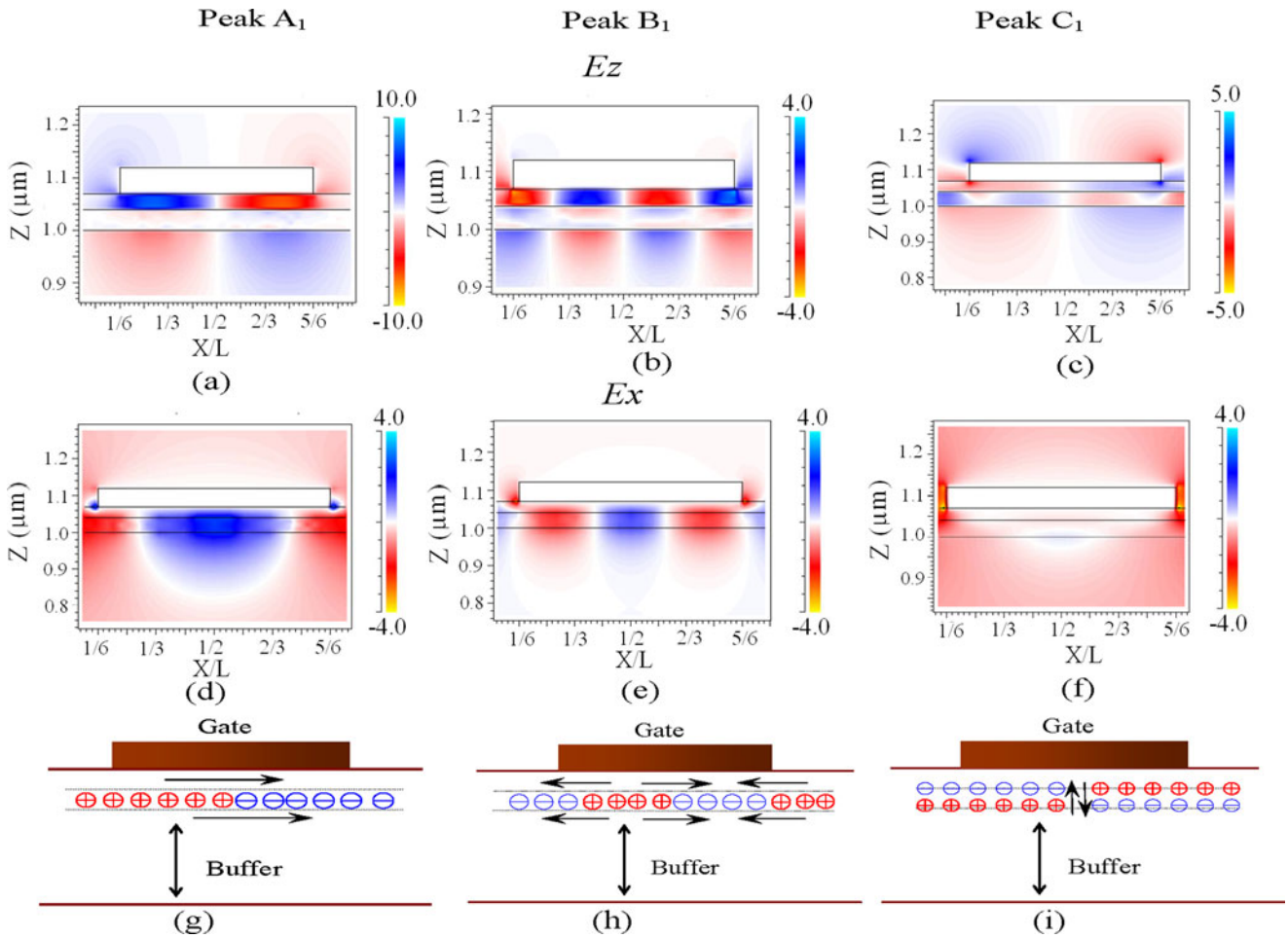

Fig. 3. Snap-shots of plasmonic oscillation and electric field distributions along the channel under the irradiation of THz wave corresponding to the frequencies of peaks A_1, B_1, and C_1. The distributions of E_z and E_x components are shown in the first and second rows, respectively. A relative coordinate *X/L* along the abscissa axis is used here and L is the structure period. The dipole distributions along the channel are also shown in the third row with respect to the electric field distributions, and the arrows show the orientation of the dipole vibrations.

Therefore, stronger absorption peak can be obtained. Referring to peak C_1 (the ASPM mode), further simulation (not shown here) indicates that it is also related to the plasmonic oscillation excited by the polarization field of the grating, e.g., the plasmon is first excited at gate edge by the polarization field, then, it experience large decay along the channel due to the asymmetrical charge distribution property and field localization in the channel (see for example [28]).

Fig. 4(a) shows the absorption properties of the device when the THz waves are incident from the back side and top side of the device. As can be seen in the data, significant damping of peak C_1 occurs when the THz wave is incident from the top side of the device. However, no significant damping can be observed for the peaks A_1 and B_1 due to the small change of the polarization field between two gate fingers. Propagation of the polarization field induced at a grating will experience decay along the surface of metal. Propagation length is reduced if the frequency of the incident field is increased. Therefore, the polarization field corresponding to the frequency of the SPM mode can propagate for a longer distance than that of the ASPM mode. Our further simulation results (not shown here) indicate that the

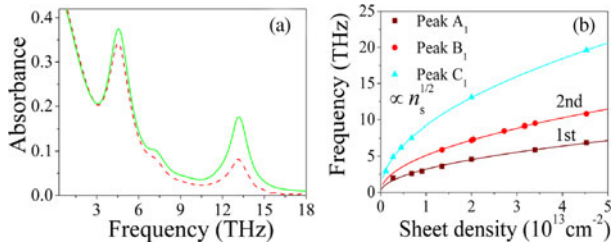

Fig. 4. (a) Absorption spectra of a metal-wire grating gate HEMT with THz wave incident from grating (red dashed line) and substrate (green solid line), the sheet electron density in the channel is 2×10^{13} cm^{-2}. (b) Fitting results of FDTD data (symbols) with formula $A\sqrt{n_s}$ for the three kind resonant peaks appearing in the spectra of metal-wire grating gate HEMT with different sheet electron densities.

ASPM plasmonic oscillation is more sensitive to the incident direction of THz waves. The strength of the polarization field between the gate fingers is much stronger (suffers less decay) when the THz wave is incident from the bottom side. Plasmonic THz absorption in grating-gate GaN HEMTs has also been well studied both experimentally and theoretically by Muravjov

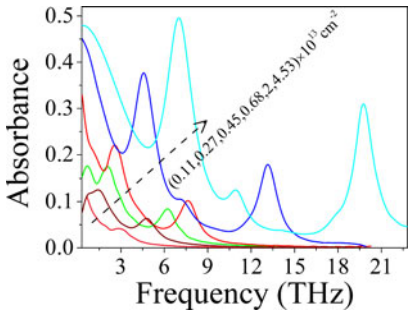

Fig. 5. Absorption spectra of metal-wire grating gate HEMT with sheet electron densities varying from 0.11 to 4.53 $\times$ 10^{13} cm^{-2}.

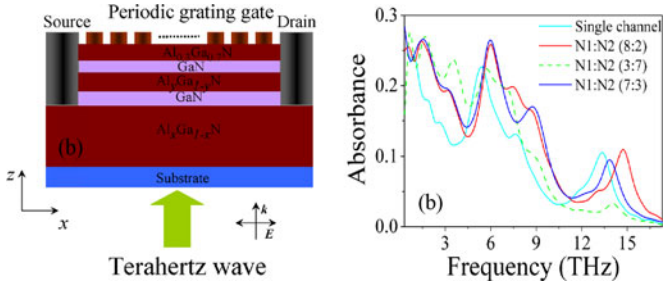

Fig. 6. (a) Schematic of the dc-HEMTs. (b) Absorption spectra of dc-HEMTs are shown under periodic sheet density modulation. The low sheet density is close to the threshold value. $N1$:$N2$ represents the ratios between the sheet densities of upper and lower channels with total densities value of $N1 + N2 =$ 3×10^{13} cm^{-2}. For comparison, the absorption spectrum of single channel HEMTs is also shown with the 2×10^{12} cm^{-2}/3×10^{13} cm^{-2} periodic electron density distributions.

et al. recently [18]. The period and slit dimensions between gate fingers in their configurations are approximately twice as large as in our devices. From their results, an absorption peak around 1.5 THz can be clearly observed at room temperature. This frequency is approximately three times smaller than that of peak A_1 showing good agreement between our results (after taking into consideration the parameters we use) and the results in [18]. However, no plasmonic absorption of the ASPM mode is observed in the results in [18]. This may be due to: 1) the weaker coupling strength between plasmon and THz radiation for larger slits; 2) the decay of polarization field since resonant frequency of ASPM mode is much higher than that of SPM mode; 3) the mode frequency goes beyond the region of the spectra in [18] (the frequency of ASPM mode is higher than 6 THz according to the results of Fig. 5 at the sheet density of 7.5×10^{12} cm^{-2}).

As compared with asymmetrical plasmonic oscillation, the field of a symmetrical plasmon spreads out of channel, interacts with the image charges in the gate, and propagates for a longer distance. The frequencies of such SPM modes satisfy the linear dispersion rule, and can be expressed as follows [7], [18], [29]:

$$\omega_{pm} \approx m\Delta\omega_1 = \sqrt{\frac{e^2 dn_s}{\varepsilon_0 \varepsilon_r m^*}} k_{pm} \tag{10}$$

where k_{pm} is plasma wave vector according to selection rule $k_{pm} = 2\pi m/a$ ($m = 1, 2, 3\ldots$), a is the period of grating-gate, $\Delta\omega_1$ is the frequency of fundamental mode ($m = 1$), d is the gate-to-channel distance, ε_0 is permittivity of free space, and ε_r is dielectric constant of barrier layer. From the fitted results in Fig. 4(b), it can be found that the relationship between the frequencies of the three peaks in the spectrum of metal wire grating gate HEMT and the sheet electron density satisfies the rule of $A\sqrt{n_s}$ [30]. Although the ratio of fitted constant between peaks A_1 and B_1 is not strictly equal to 1:2, the peak A_1 is caused by the excitation of fundamental mode and peak B_1 is caused by the second-order resonant mode. This can be concluded from the field distribution in Fig. 3(a) and (b) since the period of the structure is almost commensurate with one and two times the plasmon wavelength.

Fig. 5 shows the absorption spectra with various sheet densities. As can be seen from this figure, the fundamental plasmon resonant strength increases up to five times when the sheet density increases from 0.11 to 4.53 $\times$ 10^{13} cm^{-2}. Referring to the surface resonant layer model in Section III, there are two limiting cases for the damping of plasmons: 1) $\gamma_e \gg \gamma_{rm}$ at low electron density, where the Drude background absorption dominates, and 2) $\gamma_{rm} \gg \gamma_e$ at high electron density, where the radiative phenomenon dominates. If the electron density is changed from case (1) to (2), at first, the resonant absorption and radiative damping increase with the density change and maximum resonant absorption is reached when $\gamma_e = \gamma_{rm}$. The resonant absorption tends to be damped when the density changes to case (2). The continuous enhancement in resonant strength of these peaks in Fig. 5 is consistent with the trend described by the surface resonant layer model. The maximum absorbance 0.5 is reached at sheet density of 4.53×10^{13} cm^{-2}. A resonant-like peak at about 1 THz in the spectrum of a device with sheet density 0.45×10^{13} cm^{-2} is mainly caused by numerical errors inherent in the FDTD simulation process.

As discussed earlier, the dipole distribution is related to sheet density fluctuations and can be tuned by gate voltage. In order to achieve wider tunability, it is important to explore more advanced device structures since the forms of dipole oscillation and electromagnetic coupling can be different and even more intricate than that in a single channel system [28], [31]. For examples, the double channel HEMTs and plasmonic crystal can be utilized for this purpose [27], [28], [32]. Here, we simply present and discuss the absorption spectra of double channel HEMTs (for more information about the dynamic of plasmonic oscillation along the channel of dc-HEMT see [27]). The artificial device structure is shown in Fig. 6(a). The interchannel barrier $Al_yGa_{1-y}N$ splits the GaN channel into the upper and lower channels. The mole fraction y can be graded to a high value in order to ensure good channels isolation. The unique property of this type of device shows that more dimensional tunability can be obtained because densities of 2DEG in the two channels can be redistributed within the total sheet density by applying appropriate gate voltages (here, the total density is assumed to be 3×10^{13} cm^{-2} with the densities of the two channels combined together).

The numerical results are shown in Fig. 6(b). The sheet densities in the channels can be modulated by applying interdigitated gate voltage on the electrodes. The parts of channels with low

sheet density (2×10^{12} cm^{-2}) are modulated by the gate voltage close to the threshold condition. Other parts of the channel remain at the initial density levels (3×10^{13} cm^{-2}) but have different density distributions in the two channels. More absorption peaks can be obtained with a periodically modulated sheet density. For single channel (SC) HEMTs in Fig. 6(b), three resonant peaks locating at low THz frequencies (lower than 4 THz) can be observed, but there is only a single absorption peak in Fig. 5 at a sheet density lower than 2×10^{12} cm^{-2}.

In a dc structure, the electromagnetic interaction between adjacent channels can cause the formation of complicated plasmon modes [27]. The resonant peaks with frequencies lower than 4 THz in Fig. 6(b) are even stronger for a dc structure (the peaks in a SC structure are almost damped). Also, more absorption peaks can be observed after modulating the densities of 2DEG in the channels of dc structure. Therefore, wider tunable detection of THz wave can be realized with the dc HEMTs.

V. Conclusion

The THz resonant absorptions in grating-gate GaN HEMTs are numerically studied by using the FDTD method. The results show that HEMT devices with metal grating gates have superior resonant absorption than those with quantum wire grating gates. The dynamic response of plasmons under excitation of THz waves is investigated in detail, beyond which two types of plasmons with symmetrical and asymmetrical charge density distribution can be obtained. And the variation of plasmonic resonant strength can be described by the surface resonant layer model. These indicate that the FDTD method can be utilized for the study of coupling between THz wave and plasmons in the channel. In order to reach wider tunability in frequency, it is necessary to exploit more advanced device structures. As an example, a double channel structure can be proposed for improving the strength of THz resonance by up to 70% at frequencies lower than 4 THz (see [27]). From this point, the dc structure can be a choice for THz application.

Acknowledgment

The authors would like to thank J. Torley from the University of Colorado at Colorado Springs for critical reading of this manuscript.

References

[1] N. Pala and M. S. Shur, "Plasmonic terahertz detectors for biodetection," *Electron. Lett.*, vol. 44, pp. 1391–1392, 2008.

[2] W. Knap, M. Dyakonov, D. Coquillat, F. Teppe, N. Dyakonova, J. Lusakonski, K. Kavpierz, M. Sakowicz, G. Valusis, D. Seliuta, I. Kasalynas, A. EI Fatimy, Y. M. Meziani, and T. Otsuji, "Field effect transistors for terahertz detection: Physics and first imaging applications," *J. Infrared Milli Terahz Waves*, vol. 30, pp. 1319–1337, 2009.

[3] E. A. Shaner, A. D. Grine, J. L. Reno, M. C. Wanke, and S. J. Allen, "Next-generation detectors—Plasmon grating-gate devices have potential as tunable terahertz detectors," *Laser Focus World*, vol. 44, pp. 131–133, 2008.

[4] M. Dyakonov and M. S. Shur, "Shallow water analogy for a ballistic field effect transistor: New mechanism of plasma wave generation by dc current," *Phys. Rev. Lett.*, vol. 71, pp. 2465–2468, 1993.

[5] F. Teppe, M. Orlov, A. EI. Fatimy, A. Tiberj, W. Knap, J. Torres, V. Gavrilenko, A. Shchepetov, Y. Roelens, and S. Bollaert, "Room temperature tunable detection of subterahertz radiation by plasma waves in nanometer InGaAs transistors," *Appl. Phys. Lett.*, vol. 89, p. 222109, 2006.

[6] T. Otsuji, M. Hauable, T. Nishimara, and E. Sano, "A grating-bicoupled plasma-wave photomixer with resonant-cavity enhanced structure," *Opt. Express*, vol. 14, pp. 4815–4825, 2006.

[7] S. J. Allen, Jr., D. C. Tsui, and R. A. Logan, "Observation of two-dimensional plasmon in silicon inversion layers," *Phys. Rev. Lett.*, vol. 38, pp. 980–982, 1977.

[8] E. A. Shaner, Mark Lee, M. C. Wanke, A. D. Grine, J. L. Reno, and S. J. Allen *Appl. Phys. Lett.*, vol. 87, p. 193507, 2005.

[9] V. V. Popov, D. M. Ermolaev, K. V. Maremyanin, N. A. Maleev, V. E. Zemlyakov, V. I. Gavrilenko, and S. Yu. Shapoval, "High-responsivity terahertz detection by on-chip InGaAs/GaAs field-effect-transistor array," *Appl. Phys. Lett.*, vol. 98, p. 153504, 2011.

[10] T. A. Elkhatib, V. Yu. Kachorovskii, W. J. Stillman, D. B. Veksler, K. N. Salama, X.-C. Zhang, and M. S. Shur, "Enhanced plasma wave detection of terahertz radiation using multiple high electron-mobility transistors connected in series," *IEEE Trans. Microwave Theory Tech.*, vol. 58, no. 2, pp. 331–337, Feb. 2010.

[11] D. Veksler, F. Teppe, A. P. Dmitriev, V. Yu. Kachorovskii, W. Knap, and M. S. Shur, "Detection of terahertz radiation in gated two-dimensional structures governed by dc current," *Phys. Rev. B.*, vol. 73, p. 125328, 2006.

[12] V. V. Popov, O. V. Polischuk, and M. S. Shur, "Resonant excitation of plasma oscillations in partially gated two-dimensional electron layer," *J. Appl. Phys.*, vol. 98, p. 033510, 2005.

[13] A. EI. Fatimy, F. Teppe, N. Dyakonova, W. Knap, D. Seliuta, G. Valušis, A. Shchepetor, Y. Roelens, S. Bollaert, A. Cappy, and S. Rumyantser, "Resonant and voltage-tunable terahertz detection in InGaAs/InP nanometer transistors," *Appl. Phys. Lett.*, vol. 89, p. 131926, 2006.

[14] M. Dyakonov and M. S. Shur, "Detection, mixing, and frequency multiplication of terahertz radiation by two-dimensional electron fluid," *IEEE Trans. Electron Devices*, vol. 43, no. 3, pp. 380–387, Mar. 1996.

[15] M. S. Shur and J. Q. Lu, "Terahertz sources and detectors using two-dimensional electronic fluid in high electron-mobility transistors," *IEEE Trans. Microave Theory Tech.*, vol. 48, no. 4, pp. 750–756, Apr. 2000.

[16] V. V. Popov, O. V. Polischuk, W. Knap, and A. EI. Fatimy, "Broadening of the plasmon resonance due to plasmon-plasmon intermode scattering in terahertz high-electron-mobility transistors," *Appl. Phys. Lett.*, vol. 93, p. 263503, 2008.

[17] D. Coquillat, S. Nadar, F. Teppe, N. Dyakonova, S. Boubanga-Tombet, W. Knap, T. Nishimura, T. Otsuji, Y. M. Meziani, G. M. Tsymbalov, and V. V. Popov, "Room temperature detection of sub-terahertz radiation in double-grating-gate transistors," *Opt. Express*, vol. 18, pp. 6024–6032, 2010.

[18] A. V. Muravjov, D. B. Veksler, V. V. Popov, O. V. Polischuk, N. Pala, X. Hu, R. Gaska, H. Saxena, R. E. Peale, and M. S. Shur, "Temperature dependence of plasmonic terahertz absorption in grating-gate gallium-nitride transistor structures," *Appl. Phys. Lett.*, vol. 96, p. 042105, 2010.

[19] A. EI Fatimy, N. Dyakonova, Y. Meciani, T. Ostuji, W. Knap, S. Vandenbronk, K. Madjour, D. Théron, C. Gaquieve, M. A. Poisson, S. Delage, P. Prystawko, and C. Skierbiszewski, "AlGaN/GaN high electron mobility transistors as a voltage-tunable room temperature terahertz sources," *J. Appl. Phys.*, vol. 107, p. 024504, 2010.

[20] A. V. Muravjov, D. B. Veksler, X. Hu, R. Gaska, N. Pala, H. Saxena, R. E. Peale, M. S. Shur, "Resonant terahertz absorption by plasmons in grating-gate GaN HEMT structures," *Proc. SPIE*, vol. 7311, p. 73110D, 2009.

[21] O. Ambacher, J. Majewski, C. Miskys, A. Link, M. Hermann, M. Eickhoff, M. Stutzmann, F. Bernardini, V. Fiorentini, V. Tilak, B. Schaff, and L. F. Eastman, "Pyroelectric properties of Al(In)GaN/GaN hetro-and quantum well structures," *J. Phys.: Condens. Matter.*, vol. 14, pp. 3399–3434, 2002.

[22] S. A. Mikhailov, "Plasma wave instability and amplification of electromagnetic waves in low-dimensional electron systems," *Phys. Rev. B.*, vol. 58, pp. 1517–1531, 1998.

[23] V. V. Popov, G. M. Tsymbalov, and M. S. Shur, "Plasma instability and amplification of terahertz radiation in field-effect transistor arrays," *J. Phys: Condens. Matter.*, vol. 20, pp. 1–6, 2008.

[24] V. V. Popov, O. V. Polischuk, T. V. Teperik, X. G. Peralta, S. J. Allen, N. J. M. Horing, and M. C. Wanke, "Absorption of terahertz radiation by plasmon modes in a grid-gated double-quantum-well field-effect transistor," *J. Appl. Phys.*, vol. 94, pp. 3556–3562, 2003.

[25] V. V. Popov, D. V. Fateev, O. V. Polischuk, and M. S. Shur, "Enhanced electromagnetic coupling between terahertz radiation and plasmons in a

grating-gate transistor structure on membrane substrate," *Opt. Express*, vol. 18, pp. 16771–16776, 2010.
[26] Y. Zeng, Y. Fu, M. Bengesson, X. S. Chen, W. Lu, and H. Ågren, "Finite-difference time-domain simulations of exciton-polariton resonances in quantum-dot arrays," *Opt. Express*, vol. 16, pp. 4507–4519, 2008.
[27] L. Wang, X. S. Chen, W. D. Hu, J. Wang, J. Wang, X. D. Wang, and W. Lu, "The plasmonic resonant absorption in GaN double-channel high electron mobility transistors," *Appl. Phys. Lett.*, vol. 99, p. 063502, 2011.
[28] T. V. Teperik, F. J. García de Abajo, V. V. Popov, and M. S. Shur, "Strong terahertz absorption bands in a scaled plasmonic crystal," *Appl. Phys. Lett.*, vol. 90, p. 251910, 2007.
[29] G. C. Dyer, J. D. Crossno, G. R. Aizin, E. A. Shaner, M. C. Wanke, J. L. Reno, and S. J. Allen, "A plasmonic terahertz detector with a monolithic hot electron bolometer," *J. Phys.: Condens. Matter*, vol. 21, p. 195803, 2009.
[30] G. C. Dyer, G. R. Aizin, J. L. Reno, E. A. Shaner, and S. J. Allen, "Novel tunable millimeter-wave grating-gated plasmonic detectors," *IEEE J. Sel. Top. Quantum Electron.*, vol. 17, no. 1, pp. 85–91, Jan./Feb. 2011.
[31] X. G. Peralta, S. J. Allen, M. C. Wanke, N. E. Harff, J. A. Simmons, M. P. Lilly, J. L. Reno, P. J. Burke, and J. P. Eisenstein, "Terahertz photoconductivity and plasmon modes in double-quantum-well field-effect transistors," *Appl. Phys. Lett.*, vol. 81, pp. 1627–1629, 2002.
[32] R. M. Chu, Y. G. Zhou, J. Liu, D. L. Wang, K. J. Chen, and K. M. Lau, "AlGaN-GaN double-channel HEMTs," *IEEE Trans. Electron. Devices*, vol. 52, no. 4, pp. 438–445, Apr. 2005.

Lin Wang received the B.S. degree in applied physics (Hons.) from the Zhejiang University of Science and Technology, Hangzhou, China, in 2008. He is currently working toward the Ph.D. degree in microelectronics and solid-state electronics at the Shanghai Institute of Technical Physics, Chinese Academy of Sciences, Shanghai, China.

His current research interests include plasma wave detection of terahertz radiation and GaN-based high power device simulations.

Xiao-Shuang Chen received the Ph.D. degree in condensed matter physics from Nanjing University, Jiangsu, China, in 1995.

He has been a Research Fellow in the Korea Institute of Advanced Study, University of Tokyo, Tokyo, Japan, and Humboldt Research Fellow in Universität Würzburg, Würzburg, Germany. He has authored or coauthored more than 100 publications. He is currently a Professor in the Shanghai Institute of Technical Physics, Chinese Academy of Sciences, and the Vice Director of the National Laboratory for Infrared Physics. His current research interests include low-dimensional field-effect transistor terahertz detectors, the physics of nanoelectronic devices and photonic crystals, infrared photoelectronic materials, and device design.

Dr. Chen has won many national prizes for solving problems in infrared electronics.

Wei-Da Hu received the B.S. and M.S. degrees in material of science from the Wuhan University of Technology, Wuhan, China, in 2001 and 2004, respectively, and the Ph.D. degree (Hons.) in microelectronics and solid-state electronics from the Shanghai Institute of Technical Physics, Chinese Academy of Sciences, Shanghai, China, in 2007.

His experiences range from HgCdTe-based photodetector simulations to GaN-based devices (such as HEMT and APD) design and simulations. He is currently an Associate Professor on modeling, simulation, and design of photodetectors in the Shanghai Institute of Technical Physics. He has authored or coauthored more than 50 technical journal papers and conference presentations. His current research interests include plasma wave detection of terahertz radiation using HEMTs, GaN-based device simulations, and HgCdTe-based photodetector simulations.

Wei Lu (M'10) received the B.S. degree in physics from Fudan University, Shanghai, China, in 1983, and the Ph.D. degree from the Shanghai Institute of Technical Physics, Chinese Academy of Sciences, Shanghai, China, in 1988.

He has been the Research Fellow in the Technical University of Braunschweig, Braunschweig, Germany, 1989, and a Visiting Professor in the many countries. He is currently a Professor in Shanghai Institute of Technical Physics. He has authored or coauthored more than 150 publications on optoelectronic materials and devices. His current research interests include HgCdTe-based photodetectors, semiconductor physics and solid spectroscopy, and physics of condensed matter.

Dr. Lu is the Director of the National Laboratory for Infrared Physics and Shanghai Physical Society. He is the recipient of many national awards. He is also serving on the editorial board of the *Journal of Applied Physics*.